analytical chemistry

pubs.acs.org/ac Article

Colorimetric Cotton Swab for Viral Protease Detection

Ranit Dutta,[‖] Sparsh Makhaik,[‖] Peiyao Zhao,[‖] Kristalle G. Cruz, Kwang-Won Park, Hongxu Liu, Trisha L. Andrew,* Jeanne A. Hardy,* and S. Thayumanavan*

Cite This: https://doi.org/10.1021/acs.analchem.2c02033 Read Online

ACCESS | Metrics & More | Article Recommendations | Supporting Information

ABSTRACT: Reporting the activity of a specific viral protease remains an acute need for rapid point-of-care detection strategies that can distinguish active infection from a resolved infection. In this work, we present a simple colorimetric approach for reporting the activity of a specific viral protease through direct color conversion on a cotton swab, which has the potential to be extended to detect the corresponding virus. We use SARS-CoV-2 viral protease as a proof-of-concept model system. We use 4-aminomalachite green (4-AMG) as the base chromophore structure to design a CoV2-AMG reporter, which is selective toward the SARS-CoV-2 M^{pro} but does not produce any observable color change in the presence of other viral proteases. The color change is observable by the naked eye, as well as smartphone imaging, which affords a lower limit of detection. The simplicity and generalizability of the method could be instrumental in combating future viral outbreaks.

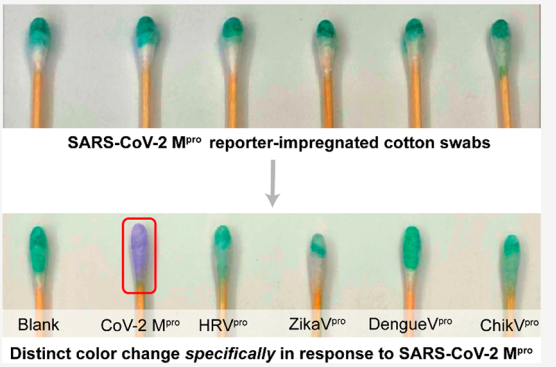

1. INTRODUCTION

Current detection methods for viral infections, such as RT-PCR, serological, antigen, and antibody-based tests,[1−3] focus on either recognizing specific components of the viral particle or host immune response affording reliable testing for identified pathogens but have limitations that hinder their deployment for emerging pathogens.[1,2,4,5] In many viral families, the genomes encode a polyprotein that is cleaved by an encoded viral protease to generate both structural and enzymatic components.[6−9] As proteases are less prone to mutation,[10] sensing proteases represents a sustainable approach to detecting viral activity. Similarly, because proteases are more labile than viral coat proteins or nucleic acids,[11,12] their activity is a direct indication of an active infection and can be used for differentiation from a resolved one. We hypothesized that a vivid color change reporting on activity of a specific viral protease could be a colorimetric reporter of an active viral infection. We were particularly interested in incorporating colorimetric reporters that are colorfast textile colorants,[13] as it lends itself to combined sample collection and detection.[14−16]

For this proof-of-concept work, we chose to construct a chromophoric reporter for SARS-CoV-2 M^{pro}, because the coronavirus outbreak remains a global health crisis, despite the availability of vaccines and antiviral drugs.[17−19] The SARS-CoV-2 M^{pro} is a homodimeric cysteine protease which shows a preference for cleaving peptide bonds after Gln in a sequence that includes Leu-Gln↓(Ser/Ala/Gly) where the ↓ represents the site of cleavage.[20,21]

2. EXPERIMENTAL SECTION

2.1. Materials and Instruments. All chemicals were directly purchased from commercial sources and used as received unless otherwise mentioned. *N*,*N*-Dimethylaniline, 1-propylphosphonic acid cyclic anhydride (T3P) (50+% w/w solution in dichloromethane), and *N*,*N*-diisopropylethylamine (DIPEA) were received from Alfa Aesar. 4-Nitrobenzaldehyde, trifluoroacetic acid (TFA), zinc, and zinc chloride were purchased from Acros Organics. Triisopropylsilane (TIPS), 2,3-dichloro-5,6-dicyano-1,4-benzoquinone (DDQ), sodium tetrafluoroborate ($NaBF_4$), Tris-HCl, phosphate buffered saline (PBS), CHAPS, NaCl, and imidazole were purchased from Sigma-Aldrich. Isopropyl β-D-1-thiogalactopyranoside and dithiothreitol (DTT) were purchased from GoldBio. All the solvents, glacial acetic acid, inorganic acids, and bases were bought from Fisher Scientific. NMR spectra for all compounds were recorded on a 400 MHz Bruker NMR spectrometer. ESI-MS data were obtained on the Bruker MicroTOF-II-ESI mass spectrometer using positive mode ionization.

2.2. Synthesis of the Colorimetric Probe (CoV2-AMG). *2.2.1. Synthesis of 4-Nitroleucomalachitegreen (1).* To a mixture of *N*,*N*-dimethylaniline (5.00 g, 41.01 mmol) and 4-

Received: May 10, 2022
Accepted: August 23, 2022

nitrobenzaldehyde (2.07 g, 13.67 mmol), $ZnCl_2$ (5.59 g, 41.01 mmol) was added, and the mixture was stirred at 100 °C for 5 h. The resultant green solution was cooled to room temperature and filtered through a fritted funnel under vacuum followed by washing with acetone. Water was added to the filtrate to promote crystallization and thereafter kept in the refrigerator overnight. The crystals were filtered again, recrystallized in butanol, and dried via rotary evaporation and in vacuo. The final product was obtained as a green solid with 81% (4.17 g) yield (Scheme 1). ^{1}H NMR (400 MHz, DMSO-d_6) δ 8.18−8.14 (td, J = 10.66 Hz, 2.66 Hz, 2H), 7.37−7.33 (td, J = 9.33 Hz, 2.66 Hz, 2H), 6.92−6.89 (m, 4H), 6.69−6.66 (m, 4H), 5.51 (s, 1H), 2.86 (s, 12H); ^{13}C NMR (100 MHz, DMSO-d_6) δ 154.1, 149.4, 146.1, 131.2, 130.5, 129.9, 123.8, 112.9, 54.3, 40.6 (Figure S8).

Scheme 1. Chemical Synthesis of CoV2-AMG

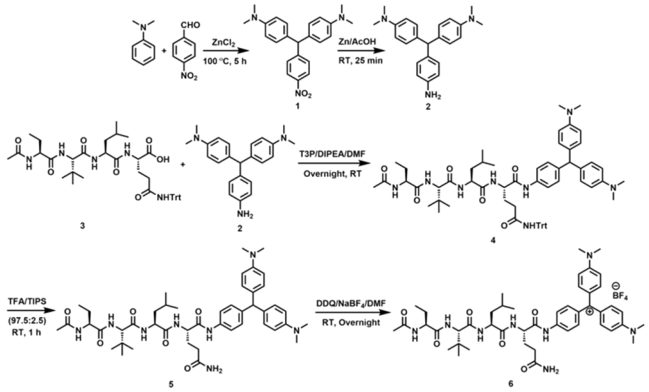

*2.2.2. Synthesis of 4-Aminoleucomalachitegreen (4-ALMG) (**2**).* Compound **1** (3.00 g, 7.99 mmol) was dissolved in the mixture of 30 mL of glacial acetic acid and 8 mL of water. 10.45 g of zinc powder (159.80 mmol) was added to the mixture and stirred at room temperature for 30 min. The reaction mixture was filtered and concentrated via rotary evaporation. The resulting reddish syrup was dissolved in chloroform and extracted with saturated $NaHCO_3$ solution (2 × 80 mL) followed by saturated NaCl solution (80 mL). The organic phase was dried over anhydrous Na_2SO_4 and further dried via rotary evaporation and in vacuo to obtain the dark brown final product **2** with 86% yield (2.38 g). ^{1}H NMR (400 MHz, DMSO-d_6) δ 6.88−6.86 (dd, J = 6 Hz, 4 Hz, 4H), 6.73−6.70 (dd, J = 8 Hz, 4 Hz, 2H), 6.63−6.60 (dd, J = 8 Hz, 4 Hz, 4H), 6.47−6.45 (dd, J = 6 Hz, 4 Hz, 2H), 5.10 (s, 1H), 4.79 (s, 2H), 2.84 (s, 12H); ^{13}C NMR (100 MHz, acetone-d_6) δ 133.7, 133.0, 129.6, 129.6, 122.3, 118.9, 114.0, 112.3, 54.2, 39.9 (Figure S8).

*2.2.3. Synthesis of Ac-Abu-Tle-Leu-Gln(Trt)-4-ALMG (**4**).* Compound **3**, i.e., Ac-Abu-Tle-Leu-Gln(Trt)-COOH peptide (50.00 mg, 0.06 mmol) was dissolved in dry DMF (0.50 mL) in the presence of 23.5 μL of DIPEA (0.13 mmol). It was then mixed with 85.77 mg of 50 wt % solution of T3P (0.13 mmol) in DCM. The mixture was stirred at room temperature for 20 min. Compound **2** (28 mg, 0.081 mmol) was dissolved in dry DMF (0.30 mL) in the presence of 11.75 μL of DIPEA and added to the previous reaction mixture. The final mixture was stirred at room temperature overnight. The solution was then diluted with DCM (8 mL) and extracted with saturated $NaHCO_3$ solution (2 × 8 mL) followed by saturated NaCl solution (8 mL). Finally, the organic phase was dried with anhydrous Na_2SO_4, concentrated via rotary evaporation, and purified by flash column chromatography using C-18 reversed-phase silica gel (10−50% MeCN with 0.1% TFA in water with 0.1% TFA as eluent) to obtain the final product **4** as a pale blue solid (26.00 mg, 36% yield). ^{1}H NMR (400 MHz, CD_3OD) δ 7.45−7.43 (d, J = 8 Hz, 2H), 7.30−7.20 (m, 15H), 7.04−7.02 (d, J = 8 Hz, 2H), 6.94−6.92 (d, J = 8 Hz, 4H), 6.74−6.72 (d, J = 8 Hz, 4H), 5.33 (s, 1H), 4.41 (s, 2H), 4.28−4.24 (m, 2H), 3.50 (s, 2H), 3.15−3.16 (m, 2H), 2.90 (s, 12H), 2.50 (m, 2H), 1.97 (s, 3H), 1.81−1.78 (t, J = 6 Hz, 2H), 1.70−1.61 (m, 6H), 1.09 (m, 1H), 1.00 (s, 9H), 0.97−0.93 (m, 3H), 0.94−0.90 (m, 6H); ^{13}C NMR (100 MHz, acetone-d_6) δ 174.6, 172.1, 171.9, 171.7, 171.3, 171.1, 149.1, 145.3, 140.8, 137.1, 132.8, 129.6, 129.1, 128.8, 127.4, 126.4, 119.1, 112.4, 69.9, 64.3, 56.5, 54.4, 53.9, 53.1, 39.8, 33.5, 32.5, 26.4, 24.7, 24.2, 22.7, 21.9, 20.1, 19.6, 9.7; ESI-MS (m/z) for $C_{65}H_{80}N_8O_6$ expected $[M + Na]^+$, 1091.61; obtained $[M + Na]^+$, 1091.36 (Figure S8).

*2.2.4. Deprotection to Achieve Ac-Abu-Tle-Leu-Gln-4-ALMG (**5**).* Compound **4** (26.00 mg, 0.02 mmol) was dissolved in 1 mL solution of 2.5% TIPS in TFA (v/v) added and stirred for 1 h at room temperature. The solution was concentrated via rotary evaporation, and the remaining TIPS/TFA mixture was evaporated in the presence of excess hexane. After drying in vacuo, the final product **5** was obtained as a pale blue solid (20.00 mg, quantitative yield). ESI-MS (m/z) for $C_{46}H_{66}N_8O_6$ expected $[M + Na]^+$, 849.50; obtained $[M + Na]^+$, 849.36 (Figure S8).

*2.2.5. Synthesis of Ac-Abu-Tle-Leu-Gln-4-AMG Tetrafluoroborate Salt (CoV2-AMG) (**6**).* Compound **5** (20.00 mg, 0.02 mmol) and DDQ (16.30 mg, 0.07 mmol) were dissolved in 0.50 mL of dry DMF, and 7.90 mg of $NaBF_4$ (0.07 mmol) was added to the mixture. The solution was stirred at room temperature overnight. The solution was dried through purging with argon gas, purified by flash column chromatography using C-18 reversed-phase silica gel (10−40% MeCN with 0.1% TFA in water with 0.1% TFA as eluent) to obtain the final product **6** as a green solid (16.60 mg, 84% yield). ESI-MS (m/z) for $C_{46}H_{65}N_8O_6^+$ expected $[M]^+$, 825.50; obtained $[M]^+$, 825.50 (Figure S8).

2.2.6. Purification of CoV2-AMG Reporter. The CoV2-AMG dye was purified using an analytical HPLC column (ZORBAX SB-Aq, Agilent, 4.5 mm × 250 mm) on a Shimadzu HPLC system using a flow rate of 0.5 mL/min in water:acetonitrile gradient varying from 10% to 80% over 70 min. 4-AMG and CoV2-AMG had similar elution times, but the use of a slow gradient and analytical scale column allowed successful separation of the desired product from the starting material.

2.3. Purification and Expression of SARS-CoV-2 M^{pro}. An expression plasmid encoding the *E. coli* codon optimized gene for SARS CoV-2 M^{pro} was provided by Prof. M. Joanne Lemieux from the University of Alberta, Canada. The procedure for expression and purification of the protease was adapted from a previously published procedure.[22] The plasmid was transformed into *E. coli* BL21 (DE3), and the bacterial culture was induced with 0.50 mM isopropyl β-D-1-thiogalactopyranoside. The protein was then expressed for 4 h at 37 °C. Cells were harvested by centrifugation for 10 min at 4695 RCF. The resulting cell pellet was suspended in a lysis buffer (20 mM Tris-HCl, pH 7.8, 150 mM NaCl, 5 mM imidazole) and lysed using a microfluidizer. Cell debris was removed by centrifugation for 50 min at 26915 RCF. The

https://doi.org/10.1021/acs.analchem.2c02033
Anal. Chem. XXXX, XXX, XXX−XXX

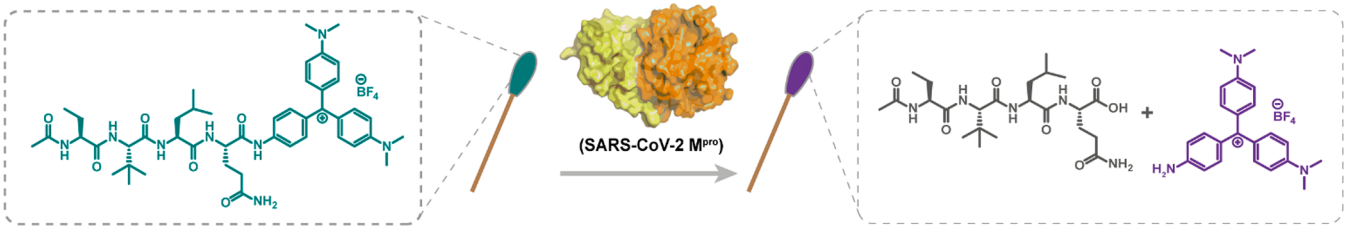

Figure 1. Design of CoV2-AMG colorimetric detection probe. The probe consists of a recognition peptide sequence for SARS-CoV-2 M^{pro},[20] attached to a chromophore 4-AMG. The color change from green to purple occurs due to cleavage of an amide bond between the Gln residue and 4-AMG by the M^{pro}.

supernatant was loaded into a HisTrap 5 mL column (Cytiva) in 20 mM Tris pH 7.8, 20 mM NaCl, 1 mM DTT. After loading the supernatant, the column was washed with approximately 25 column volumes of lysis buffer supplemented with 20 mM imidazole. Lastly, the protease was eluted from the column using an imidazole gradient of 40−500 mM imidazole. Eluted fractions were analyzed by sodium dodecyl sulfate−polyacrylamide gel electrophoresis (Figure S5). Fractions containing the pure protease were pooled. The pooled fractions were digested with His-tagged SUMO protease (McLab, South San Francisco, CA) overnight at 4 °C to remove the SUMO tag. The next day, any precipitate formed was removed by centrifugation and filtration using Millex-HP syringe filter units (0.45 μm pore size, polyethersulfone membrane, 33 mm diameter). The sample was again passed through a HisTrap column. The eluate, which contains the untagged protease, was collected. SARS CoV-2 M^{pro} was further purified using size exclusion chromatography (HiLoad Superdex 75 Prep grade 26/60, Cytiva). The activity of purified SARS CoV-2 M^{pro} was tested against the Ac-Abu-Tle-Leu-Gln-ACC substrate (Vivitide) (Figure S6).

2.4. UV Analysis of CoV2-AMG before and after Cleavage by SARS-CoV-2 M^{pro}. Different concentrations of SARS-CoV-2 M^{pro} were added to 200 μM CoV2-AMG (in PBS, pH 7.4). The absorbance spectrum and its absorbance values at 590 and 620 nm were measured after 60 min. For the time-dependent study, 2.5 μM protease was added to 200 μM CoV2-AMG (in PBS buffer pH 7.4) and the absorbance spectrum together with the absorbance values at 590 and 620 nm was measured every 15 min. All absorbance measurements were collected using SpectraMax-M5 multimode microplate reader (Molecular Devices LLC) at 25 °C.

2.5. LC−MS Analysis of CoV2-AMG Following Cleavage by SARS-CoV-2 M^{pro}. The CoV2-AMG reporter was dissolved in ethylene glycol to make a stock solution of 20 mM concentration. For determining the cleavage pattern of CoV2-AMG reporter by SARS-CoV-2 M^{pro}, time dependent LC−MS analysis was carried out at four different time intervals. A total of 50 μL solution was prepared by incubating 200 μM CoV2-AMG reporter with 2.5 μM enzyme for 30 s, 2 min, 10 min, and 30 min each. 10 μL of reaction mixture was diluted with 90 μL of 0.1% formic acid solution before injecting onto the LC−MS instrument. This also helped in quenching the reaction. All experiments were performed using Bruker SolariX FT-ICR equipped with electron ionization spray (ESI). The mass spectrometer was calibrated in positive mode using NaTFA (0.05−0.10 mg/mL in 50:50 ACN/H2O). The data were acquired and processed using Bruker Compass DataAnalysis 5.0 software (Bruker, Germany). The samples were run in water (0.1% formic acid) and acetonitrile (0.1% formic acid), the concentration of acetonitrile varying from 20% to 80% over 45 min. Full-scan MS data were acquired for a mass range of m/z 0−1500 using the positive ion mode. The LC spectra were analyzed for required peaks and plotted using MS-excel for better comparison (Figures S2 and S3).

2.6. Selectivity of CoV2-AMG for SARS-CoV-2 M^{pro} over Other Viral Proteases. The CoV2-AMG reporter was dissolved in ethylene glycol to make a stock solution of 20 mM. For determining the selectivity in solution phase, the CoV2-AMG reporter (with the final concentration of 200 μM) was incubated with different viral proteases (each at a final concentration of 10 μM) in their respective activity buffers for 30 min in a 96-well microplate. The final volume in each well was 100 μL. As a negative control, CoV2-AMG was also incubated in each activity buffer in the absence of any viral proteases. The proteases tested included human rhinovirus 3C protease (HRV^{pro}), Zika virus protease NS2B-NS3 ($ZikaV^{pro}$), dengue virus NS2B-NS3 protease ($DengueV^{pro}$), and chikungunya virus nsP2 protease ($ChikV^{pro}$). SARS-CoV-2 M^{pro} was incubated with CoV2-AMG in 1× PBS at pH-7, HRV^{pro} was incubated in a buffer containing 50 mM HEPES, 0.1 mM DTT, 150 mM NaCl at pH 7.5, $ZikaV^{pro}$ and $DengueV^{pro}$ were incubated in 10 mM Tris, 20% glycerol, 10 mM CHAPS at pH 8.5, and $ChikV^{pro}$ was incubated in buffer containing 50 mM Tris, 1 mM CHAPS, 10 mM DTT at pH 7.5. The color change was observed by the naked eye after a 30 min incubation.

For testing the selectivity on cotton swabs, the swabs were soaked in a 1 mM solution of CoV2-AMG in ethylene glycol. These swabs were allowed to dry and further incubated in solutions of different proteases at 20 μM. As a negative control, a cotton swab was incubated in the PBS without any protease. The development of change in color was observed by the naked eye after 30 min incubation. To test the effect of presence of HRV^{pro} on the selectivity of substrate, a sample of 20 μM SARS-CoV-2 M^{pro} was spiked with 2 μM HRV^{pro}. The color change in the cotton swab incubated with this sample was observed after 30 min by the naked eye. As a positive control, a cotton swab was also incubated with SARS-CoV-2 M^{pro} only, at the same concentration.

2.7. Colorimetric Quantification Assay of Viral Protease. The cotton swab was presoaked in 1 mM solution of CoV2-AMG and allowed to dry for 10 min at room temperature. These swabs were then incubated in SARS-CoV-2 M^{pro} protease solution with different concentrations (0 μM, 1 μM, 5 μM, 10 μM, 20 μM, 30 μM, 40 μM) for 30 min. All the test images of the colorimetric swab sensor were recorded using a smartphone (iPhone 11pro) at the same distance, perpendicular to the cotton swab. All images were taken against a white background with consistent ambient lighting without a camera flash. After digitalization, images were filtered and converted to CIE L*a*b* color space on MATLAB version R2018b (MathWorks, Inc.). The region of interest

https://doi.org/10.1021/acs.analchem.2c02033
Anal. Chem. XXXX, XXX, XXX−XXX

(ROI) with a radius of 0.5 cm was extracted on cotton swab images, and colorimetry data were obtained from averaging the ROI of the pixel intensity of a* and b* channels.

3. RESULTS AND DISCUSSION

3.1. Design of Peptide-Based Protease Reporter. Protease recognition sequences have been used to design fluorogenic reporters[20,23−25] but not in the context of point-of-care self-administered diagnostics. For example, we were unsuccessful in reading out fluorogenic responses generated by a commercially available fluorogenic reporter immobilized on a swab because of background scattering and autofluorescence (Figure S1). Hence, we selected 4-amino malachite green (4-AMG), which belongs to the family of cationic triarylmethane dyes that interact strongly with cotton and other textiles, eliminating the need of added binding agents or reactive chemistries for affordable, color-fast dyeing.[26,27] Based on early genome sequences of SARS-CoV-2, we predicted sequences that would be recognized by SARS-CoV-2 M^{pro} which include Leu-Gln↓(Ser/Ala/Gly).[28−30] The selected optimal peptide recognition sequence Ac-Abu-Tle-Leu-Gln-COOH [20] was functionalized at the C-terminus with 4-AMG (Figure 1). We first coupled the peptide with 4-amino-leucomalachite green (4-ALMG), which lacks the extended conjugation in 4-AMG. The product was then oxidized to obtain an intense green-colored peptide substrate: Ac-Abu-Tle-Leu-Gln-4-AMG (CoV2-AMG).

3.2. SARS-CoV-2 M^{pro} Effectively Cleaves COV2-AMG. To test cleavage efficacy and kinetics, the CoV2-AMG reporter was dissolved in PBS buffer (pH 7.4) and incubated with SARS-CoV-2 M^{pro}. Time-dependent LC−MS analyses allowed the characterization of the reporter conversion (retention time of 1395 s, MW of 825.50 Da) to the products Ac-Abu-Tle-Leu-Gln-COOH (retention time of 235 s, MW of 499.61 Da) and 4-AMG (retention time of 1431 s, MW of 344.48 Da), within just 30 s after SARS-CoV-2 M^{pro} addition (Figures 2 and S2). Replicate LC−MS measurements were performed at 1 min, 5 min, and 20 min, respectively, exhibiting a systematic increase of products and decrease of CoV2-AMG concentration. A minor additional peak was observed for the synthesized CoV2-AMG (at 1350 s), which we were unable to separate during HPLC purification. We conclude that this arises from a diastereomer of CoV2-AMG (MW 825.50 Da) which is incompatible with protease cleavage because it will not fit within the active site of the protease which is composed of all native L amino acids,[31] as the area under this peak remains nearly unchanged throughout the time course.

3.3. Cleavage of CoV2-AMG by SARS-CoV-2 M^{pro} Yields a Colorimetric Change. In addition to being cleaved as designed, the apparent color of the CoV2-AMG was observed to change from green to purple after incubation with SARS-CoV-2 M^{pro} (Figure 3a). CoV2-AMG exhibited a UV−vis absorption maximum (λ_{max}) at 620 nm at pH 7.4 in PBS buffer. Upon exposure to the protease, this peak decreased in intensity with a concomitant appearance of a new band at λ_{max} 590 nm (Figure 3b,c), consistent with the observed color change. On a molecular level, we posit that a donor−acceptor interaction between the electron-rich dimethylanilines and the electron-deficient amide of the reporter is disrupted upon protease cleavage, as the amide is converted to a more electron-rich primary amine in the 4-AMG chromophore as has been demonstrated previously.[32]

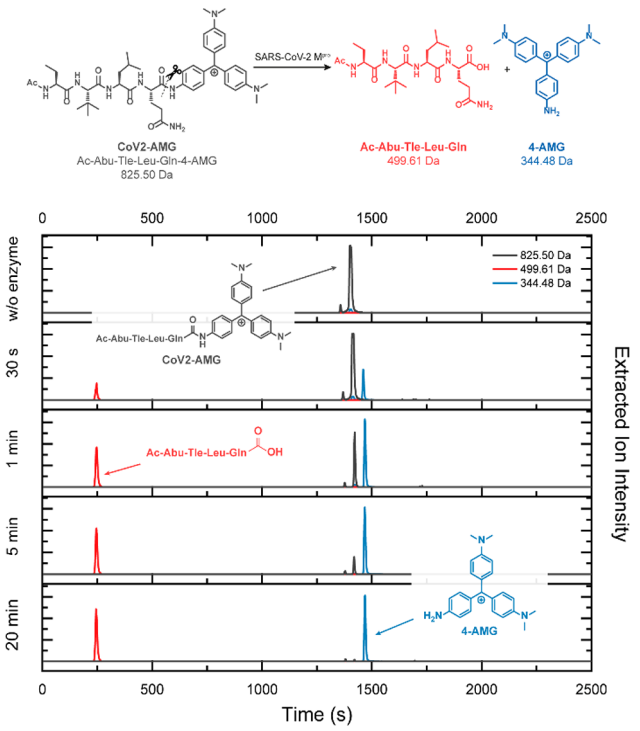

Figure 2. SARS-CoV-2 M^{pro} cleaves the CoV2-AMG after the Gln residue. The reporter cleavage reaction was monitored using LC−MS after the addition of the protease (2.5 μM) to the substrate (200 μM) over the course of 20 min. The appearance of a peak for Ac-Abu-Tle-Leu-Gln-COOH and 4-amino malachite green correlates with the disappearance of CoV2-AMG.

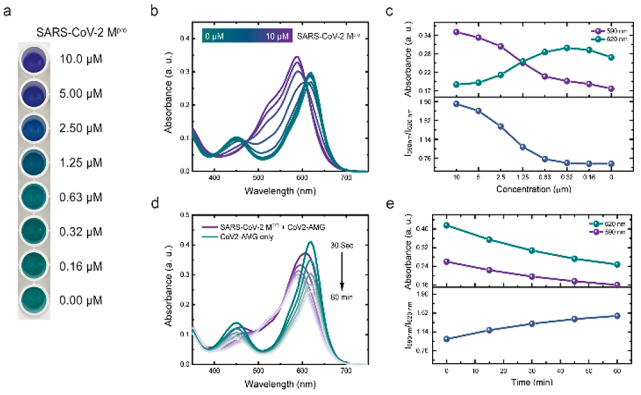

Figure 3. UV−visible absorbance properties of CoV2-AMG in the presence of SARS-CoV-2 M^{pro}. (a) Digital photograph of CoV2-AMG (200 μM) in PBS buffer with increasing concentrations of SARS-CoV-2 M^{pro}. (b) Corresponding UV−vis absorption spectra of CoV2-AMG with increasing concentrations of SARS-CoV-2 M^{pro}. (c) Absorbance intensity changes of CoV2-AMG at λ = 590 and 620 nm (top) and relative intensity (bottom) were observed as a function of SARS-CoV-2 M^{pro} concentration. (d) Time course depicting the changes to the UV−vis absorption spectra of CoV2-AMG (200 μM) in the absence (green) or presence (purple) of SARS-CoV-2 M^{pro} (2.5 μM). Absorbance values were acquired every 15 min. Approximately 30 s elapsed after addition of SARS-CoV-2 M^{pro} to the sample prior to the initial measurement during which a significant shift in λ_{max} was observed. (e) Corresponding plots of absorbance at λ = 590 and 620 nm (top) and relative intensity (bottom) as a function of time.

Time-dependent measurements revealed a rapid conversion of the absorbance band from 620 to 590 nm within the first 30

https://doi.org/10.1021/acs.analchem.2c02033
Anal. Chem. XXXX, XXX, XXX−XXX

s after addition of the SARS-CoV-2 M^{pro}, which is consistent with the LC−MS data. A steady-state absorbance intensity was gradually reached at longer time points (Figure 3d,e). The absorbance of both the intact and cleaved CoV2-AMG reporter appeared to be sensitive to photobleaching as a function of time, but this decreased intensity did not impact the overall performance of the reporter. The limit of detection for the protease with this first-generation reporter appeared to be <2.50 μM by the naked eye (Figure 3a), while ratiometric analysis revealed a more sensitive detection limit of ≤1.25 μM (Figure 3c).

3.4. Solid-State Colorimetric Viral Detection Using Cotton Swabs. Sensors based on protein−cellulose systems for colorimetric detection have been reported for diagnostic purposes due to high absorbance characteristics of cellulose.[33−36] These intrinsic properties of cotton (cellulose) allow for the entrapment of chromophore substrates while enabling retention of enzymatic activity upon mild dehydration and varying pH conditions. Thus, cotton swabs can be used as a point-of-care diagnostic method without necessitating pretreatment steps. To demonstrate the swab-based colorimetric sensors, the CoV2-AMG substrates were immobilized onto cotton swabs. In addition, the CIE color coordinates were examined from the smartphone images for quantitative analysis (Figure 4a,b). The CIE color space is device-independent; i.e.,

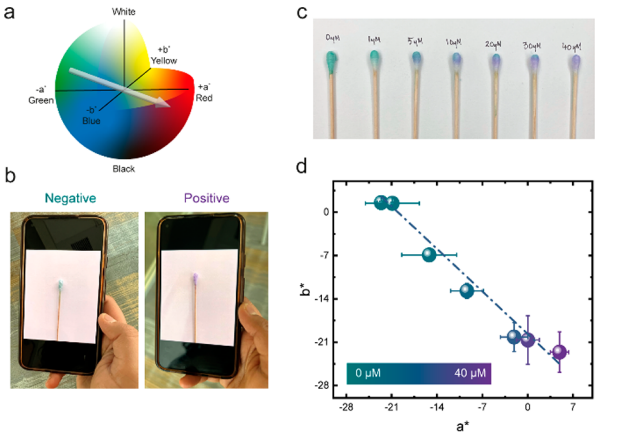

Figure 4. CIE color coordinates for color change due to the cleavage of CoV2-AMG. (a) CIE color coordinate (the white arrow indicates the color transition before and after the protease−peptide reaction). (b) Smartphone image capturing the colorimetric cotton swabs for digital interpretation. (c) Digital photograph of CoV2-AMG loaded cotton swabs 10 min after reacting with increasing concentrations of SARS-CoV-2 M^{pro}. (d) Corresponding plot of a* and b* values extracted from the CIE color coordinate of smartphone images of the CoV2-AMG swabs.

it does not change with varying photodetector or display systems and is therefore more useful for detecting weaker color changes caused by lower viral protease concentrations.

After adding SARS-CoV-2 M^{pro}, the CoV2-AMG loaded cotton swabs showed a color change from green to purple, which was more significant with increasing protease concentration and was easily observed with the naked eye within 10 min of incubation (Figure 4c). The color in the CIE system can be presented as three values: L* as lightness and a* and b* expressing red, green, blue, and yellow colors. For quantitative analysis, L*, a*, and b* parameters were acquired from the region of interest of the cotton swab. With increasing protease concentration, a* changed from negative value to positive (color transition from green to red), while b* changed from positive to negative (color change from blue to yellow). Therefore, the color changes were more comparable when the CIE values were plotted in a*b* coordinates. The limit of detection of this method was found to be ∼5 μM, where a transition from green to purple appeared, as indicated in the center point (Figure 4d).

3.5. Selectivity of CoV2-AMG toward SARS-CoV-2 M^{pro}. To assess the selectivity of our reporter platform, the CoV2-AMG detection probe was incubated with several other viral endoproteases from both the serine and cysteine protease families. Equal concentrations (10 μM) of four different enzymes, namely, human rhinovirus 3C protease (HRV^{pro}), Zika virus NS2B-NS3 protease ($ZikaV^{pro}$), dengue virus NS2B-NS3 protease ($DengueV^{pro}$), and chikungunya virus protease nsP2 ($ChikV^{pro}$), were incubated with CoV2-AMG in their respective activity assay buffers.[37−40] A vivid color change from green to purple was observed within 5 min of protease addition exclusively in the case of SARS-CoV-2 M^{pro} (Figure 5a); however, the image was captured after a 30 min incubation to capture any additional changes that might have occurred.

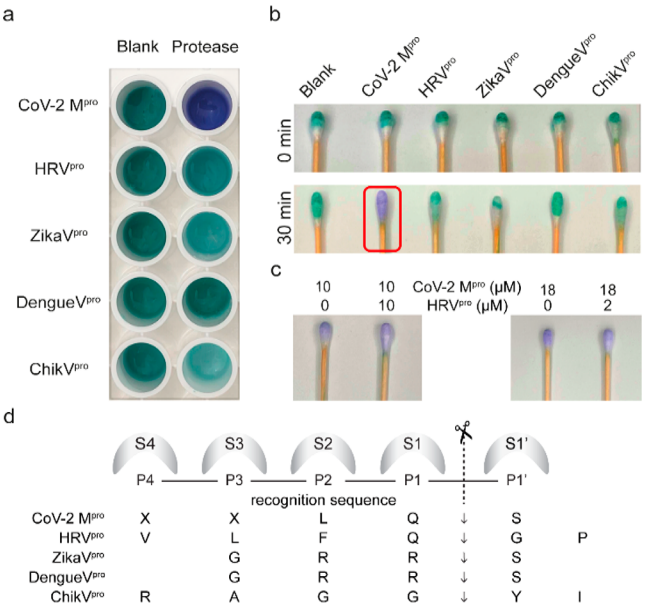

Figure 5. Selectivity of CoV2-AMG toward SARS-CoV-2 M^{pro}. (a) Digital photograph of CoV2-AMG (200 μM) in the presence of different viral proteases (10 μM). (b) Digital photograph of cotton swabs loaded with CoV2-AMG before (top) and after (bottom) addition of different viral proteases following a 30 min incubation. (c) Cotton swabs loaded with CoV2-AMG incubated with samples of SARS-CoV-2-M^{pro} spiked with two different concentrations of HRV^{pro} (1:1) and (9:1). (d) Schechter and Berger nomenclature for the substrate specificity that has been observed for the interrogated proteases.[37−40,42] The subsites (S) on the protease recognize the peptide residues (P) within the substrate. Proteolytic cleavage occurs between P1 and P1′ positions.

Although a slight fading of color was noted for $ChikV^{pro}$, which can be attributed to the presence of DTT in its activity buffer, it is still noteworthy that, here too, no color shift from green to purple was observed. These proteases were also incubated with cotton swabs absorbed with CoV2-AMG under identical conditions. After 10 min of incubation, the color

https://doi.org/10.1021/acs.analchem.2c02033
Anal. Chem. XXXX, XXX, XXX−XXX

change from blue to purple was observed only for SARS-CoV-2 M^{pro} (Figure 5b).

These results show the selectivity of CoV2-AMG toward SARS-CoV-2 M^{pro} since the sequence of this peptide (Ac-Abu-Tle-Leu-Gln↓) can be selectively recognized by this enzyme. HRV^{pro} also shows a preference for Gln residue at the P1 position although its overall recognition sequence differs from SARS-CoV-2 M^{pro} (Figure 5d).[37] Although we saw no activity of HRV^{pro} against the CoV2-AMG reporter (Figure 5b), we tested whether HRV^{pro} might cross-react during an assessment of SARS-CoV-2 M^{pro} activity. CoV2-AMG samples of SARS-CoV-2 M^{pro} were spiked with HRV^{pro} at two different ratios (1:1, 9:1). The SARS-CoV-2 M^{pro} mediated color change was observed in both cases. The intensity of purple color was slightly lower when both proteases were present at a 1:1 ratio (Figure 5c), but we observed no added cleavage that could be attributed to HRV^{pro}. These data clearly show that color change is evident only in the presence of SARS-CoV-2 M^{pro} and is not affected by the presence of HRV^{pro}, even though both cleave after Gln residues. Additionally, the CoV2-AMG loaded swab did not show any color change when treated with fetal bovine serum (Figure S3), further highlighting the strong specificity of the CoV2-AMG reporter to SARS-CoV-2 M^{pro}.

4. CONCLUSION

A new approach to biosensor fabrication for viral protease detection with point-of-care potential is demonstrated here. This work represents a proof-of-concept of this portable reporter, which couples the AMG chromophore with the Ac-Abu-Tle-Leu-Gln peptide that is specifically processed by SARS-CoV-2 M^{pro}. To date, we know of no studies that have successfully quantified the levels of SARS-CoV-2 M^{pro} present in various patient fluids. This technology may provide an effective means for quantifying the levels of active SARS-CoV-2 M^{pro} protein in various patient samples. Moreover, given our ability to predict the recognition sequences for other viral proteases from initial viral genome sequencing, and the replaceable nature of protease recognition sequences with various warheads and fluorophores,[41] we expect it to likewise be straightforward to predict a functional peptide for fabricating new AMG-based reporters for emerging viruses at the onset of the next outbreak. Our reporter demonstrates selectivity for detecting SARS-CoV-2 M^{pro} over other known viral proteases, including HRV^{pro} which also cleaves after Gln within the recognition sequence. The limit of detection of our current reporter is not yet comparable in sensitivity to other methods of virus detection, which will be the focus of future research especially because this strategy holds the promise of readily differentiating an active infection from a resolved infection. Overall, we report a generalizable, new approach for point-of-care detection of viral infection using protease as the detectable entity that is inexpensive and the readout to which can be readily translated to cell phone imaging, making its application convenient and global.

■ ASSOCIATED CONTENT

Supporting Information

The Supporting Information is available free of charge at https://pubs.acs.org/doi/10.1021/acs.analchem.2c02033.

Materials, methods, and characterization data (PDF)

■ AUTHOR INFORMATION

Corresponding Authors

Trisha L. Andrew − *Department of Chemistry and Department of Chemical Engineering, University of Massachusetts Amherst, Amherst, Massachusetts 01003, United States;* orcid.org/0000-0002-8193-2912; Email: tandrew@umass.edu

Jeanne A. Hardy − *Department of Chemistry, University of Massachusetts Amherst, Amherst, Massachusetts 01003, United States;* orcid.org/0000-0002-3406-7997; Email: hardy@chem.umass.edu

S. Thayumanavan − *Department of Chemistry and Department of Biomedical Engineering, University of Massachusetts Amherst, Amherst, Massachusetts 01003, United States;* orcid.org/0000-0002-6475-6726; Email: thai@umass.edu

Authors

Ranit Dutta − *Department of Chemistry, University of Massachusetts Amherst, Amherst, Massachusetts 01003, United States*

Sparsh Makhaik − *Department of Chemistry, University of Massachusetts Amherst, Amherst, Massachusetts 01003, United States*

Peiyao Zhao − *Department of Chemical Engineering, University of Massachusetts Amherst, Amherst, Massachusetts 01003, United States*

Kristalle G. Cruz − *Department of Chemistry, University of Massachusetts Amherst, Amherst, Massachusetts 01003, United States*

Kwang-Won Park − *Department of Chemistry, University of Massachusetts Amherst, Amherst, Massachusetts 01003, United States;* orcid.org/0000-0002-2700-7005

Hongxu Liu − *Department of Chemistry, University of Massachusetts Amherst, Amherst, Massachusetts 01003, United States;* orcid.org/0000-0003-0076-1259

Complete contact information is available at: https://pubs.acs.org/10.1021/acs.analchem.2c02033

Author Contributions

‖R.D., S.M., and P.Z. contributed equally.

Notes

The authors declare no competing financial interest.

■ ACKNOWLEDGMENTS

This material is based upon work supported by the Chemical Measurement and Imaging Program in the National Science Foundation Division of Chemistry under Grant No. CHE-2029416. We thank Prof. Joanne Lemieux and Jimmy Lu, University of Alberta, for the plasmid and SARS-CoV-2 M^{pro} purification protocol. We also acknowledge Cedric Bobst of the University of Massachusetts Mass Spectrometry Center (RRID:SCR_019063) for his guidance in obtaining and processing LC−MS data and Nathanael Kuzio and Andrew J. Smith of Department of Chemistry, University of Massachusetts Amherst, for their help with protein purification and activity assays.

■ REFERENCES

(1) Cassedy, A.; Parle-McDermott, A.; O'Kennedy, R. *Front. Mol. Biosci.* **2021**, *8*, 637559.

(2) Ozer, T.; Geiss, B. J.; Henry, C. S. *J. Electrochem. Soc.* **2020**, *167* (3), 037523.
(3) Kevadiya, B. D.; Machhi, J.; Herskovitz, J.; Oleynikov, M. D.; Blomberg, W. R.; Bajwa, N.; Soni, D.; Das, S.; Hasan, M.; Patel, M.; Senan, A. M.; Gorantla, S.; McMillan, J. E.; Edagwa, B.; Eisenberg, R.; Gurumurthy, C. B.; Reid, S. P. M.; Punyadeera, C.; Chang, L.; Gendelman, H. E. *Nat. Mater.* **2021**, *20* (5), 593−605.
(4) Liu, G.; Rusling, J. F. *ACS Sensors* **2021**, *6* (3), 593−612.
(5) Procop, G. W.; Kadkhoda, K.; Rhoads, D. D.; Gordon, S. G.; Reddy, A. J. *Cleveland Clin. J. Med.* **2021**, 1−7.
(6) Naqvi, A. A. T.; Fatima, K.; Mohammad, T.; Fatima, U.; Singh, I. K.; Singh, A.; Atif, S. M.; Hariprasad, G.; Hasan, G. M.; Hassan, M. I. *Biochim. Biophys. Acta - Mol. Basis Dis.* **2020**, *1866* (10), 165878.
(7) Yao, N.; Reichert, P.; Taremi, S. S.; Prosise, W. W.; Weber, P. C. *Structure* **1999**, *7* (11), 1353−1363.
(8) Shin, G.; Yost, S. A.; Miller, M. T.; Elrod, E. J.; Grakoui, A.; Marcotrigiano, J. *Proc. Natl. Acad. Sci. U. S. A.* **2012**, *109* (41), 16534−16539.
(9) Yost, S. A.; Marcotrigiano, J. *Curr. Opin. Virol.* **2013**, *3* (2), 137−142.
(10) Gorkhali, R.; Koirala, P.; Rijal, S.; Mainali, A.; Baral, A.; Bhattarai, H. K. *Bioinform. Biol. Insights* **2021**, *15*, 1−32.
(11) Narayanan, A.; Wu, X.; Yang, Z. R. *Bioinformatics* **2002**, *18*, S5−S13.
(12) Baleriola, C.; Johal, H.; Jacka, B.; Chaverot, S.; Bowden, S.; Lacey, S.; Rawlinson, W. *J. Clin. Microbiol.* **2011**, *49* (9), 3163−3167.
(13) Eissa, S.; Zourob, M. *Anal. Chem.* **2021**, *93* (3), 1826−1833.
(14) Alamer, S.; Eissa, S.; Chinnappan, R.; Zourob, M. *Microchim. Acta* **2018**, *185* (3), 164.
(15) Ventura, B. D.; Cennamo, M.; Minopoli, A.; Campanile, R.; Censi, S. B.; Terracciano, D.; Portella, G.; Velotta, R. *ACS Sens.* **2020**, *5* (10), 3043−3048.
(16) Ferreira, A. L.; De Lima, L. F.; Torres, M. D. T.; De Araujo, W. R.; De La Fuente-Nunez, C. *ACS Nano* **2021**, *15* (11), 17453−17462.
(17) Hu, B.; Guo, H.; Zhou, P.; Shi, Z. L. *Nat. Rev. Microbiol.* **2021**, *19* (3), 141−154.
(18) Hui, D. S.; I Azhar, E.; Madani, T. A.; Ntoumi, F.; Kock, R.; Dar, O.; Ippolito, G.; Mchugh, T. D.; Memish, Z. A.; Drosten, C.; Zumla, A.; Petersen, E. *Int. J. Infect. Dis.* **2020**, *91*, 264−266.
(19) Venkadapathi, J.; Govindarajan, V. K.; Sekaran, S.; Venkatapathy, S. *Front. Mol. Biosci.* **2021**, *8*, 637378.
(20) Rut, W.; Groborz, K.; Zhang, L.; Sun, X.; Zmudzinski, M.; Pawlik, B.; Wang, X.; Jochmans, D.; Neyts, J.; Młynarski, W.; Hilgenfeld, R.; Drag, M. *Nat. Chem. Biol.* **2021**, *17* (2), 222−228.
(21) Zhang, L.; Lin, D.; Sun, X.; Curth, U.; Drosten, C.; Sauerhering, L.; Becker, S.; Rox, K.; Hilgenfeld, R. *Science (80-.).* **2020**, *368* (6489), 409−412.
(22) Vuong, W.; Khan, M. B.; Fischer, C.; Arutyunova, E.; Lamer, T.; Shields, J.; Saffran, H. A.; McKay, R. T.; van Belkum, M. J.; Joyce, M. A.; Young, H. S.; Tyrrell, D. L.; Vederas, J. C.; Lemieux, M. J. *Nat. Commun.* **2020**, *11* (1), 4282.
(23) Ding, X.; Ge, D.; Yang, K. L. *Sensors Actuators, B Chem.* **2014**, *201*, 234−239.
(24) Kanaoka, Y. *Angew. Chem., Int. Ed. Engl.* **1977**, *16* (3), 137−147.
(25) Stennicke, H. R.; Salvesen, G. S. *Methods* **1999**, *17* (4), 313−319.
(26) Swan, N. B.; Zaini, M. A. A. *Ecol. Chem. Eng. S* **2019**, *26* (1), 119−132.
(27) Bünemann, H.; Dattagupta, N.; Schuetz, H. J.; Muller, W. *Biochemistry* **1981**, *20* (10), 2864−2874.
(28) Hilgenfeld, R. *FEBS J.* **2014**, *281* (18), 4085−4096.
(29) Mengist, H. M.; Dilnessa, T.; Jin, T. *Front. Chem.* **2021**, *9*, 622898.
(30) Ihssen, J.; Faccio, G.; Yao, C.; Sirec, T.; Spitz, U. *STAR Protoc.* **2021**, *2* (3), 100793.
(31) Brooks, W. H.; Guida, W. C.; Daniel, K. G. *Curr. Top. Med. Chem.* **2011**, *11* (7), 760−770.
(32) Yang, X. F.; Wang, H. *Spectrochim. Acta - Part A Mol. Biomol. Spectrosc.* **2006**, *65* (5), 1063−1068.
(33) Wang, W.; Wu, W. Y.; Wang, W.; Zhu, J. J. *J. Chromatogr. A* **2010**, *1217* (24), 3896−3899.
(34) Raji, M. A.; Chinnappan, R.; Shibl, A.; Suaifan, G.; Weber, K.; Cialla-May, D.; Popp, J.; El Shorbagy, E.; Al-Kattan, K.; Zourob, M. *Talanta* **2021**, *225*, 121946.
(35) Promphet, N.; Rattanawaleedirojn, P.; Siralertmukul, K.; Soatthiyanon, N.; Potiyaraj, P.; Thanawattano, C.; Hinestroza, J. P.; Rodthongkum, N. *Talanta* **2019**, *192*, 424−430.
(36) Wang, J.; Bowie, D.; Zhang, X.; Filipe, C.; Pelton, R.; Brennan, J. D. *Chem. Mater.* **2014**, *26* (5), 1941−1947.
(37) Abdelkader, E. H.; Otting, G. *J. Biotechnol.* **2021**, *325*, 145−151.
(38) Hill, M. E.; Kumar, A.; Wells, J. A.; Hobman, T. C.; Julien, O.; Hardy, J. A. *ACS Chem. Biol.* **2018**, *13* (9), 2398−2405.
(39) Hill, M. E.; Yildiz, M.; Hardy, J. A. *Biochemistry* **2019**, *58* (6), 776−787.
(40) Singh, H.; Mudgal, R.; Narwal, M.; Kaur, R.; Singh, V. A.; Malik, A.; Chaudhary, M.; Tomar, S. *Biochimie* **2018**, *149*, 51−61.
(41) Powers, J. C.; Asgian, J. L.; Ekici, Ö. D.; James, K. E. *Chem. Rev.* **2002**, *102* (12), 4639−4750.
(42) Schechter, I.; Berger, A. *Biochem. Biophys. Res. Commun.* **1967**, *27* (2), 157−162.

https://doi.org/10.1021/acs.analchem.2c02033
Anal. Chem. XXXX, XXX, XXX−XXX